CHEMPUBSOC EUROPE

Check for updates

▌ Porous Organic Polymers

Self-Assembled, Fluorine-Rich Porous Organic Polymers: A Class of Mechanically Stiff and Hydrophobic Materials

Soumya Mukherjee+,[a] Zhixin Zeng+,[b] Mandar M. Shirolkar,[c, d] Partha Samanta,[a] Abhijeet K. Chaudhari,[b] Jin-Chong Tan,*[b] and Sujit K. Ghosh*[a, e]

Abstract: Fluorous organic building blocks were utilized to develop two self-assembled, hydrophobic, fluorinated porous organic polymers (FPOPs), namely, **FPOP-100** and **FPOP-101**. Comprehensive mechanical analyses of these functionalised triazine network polymers marked the introduction of mechanical stiffness among all porous organic network materials; the recorded stiffnesses are analogous to those of their organic–inorganic hybrid polymer congeners, that is, metal–organic frameworks. Furthermore, this study introduces a new paradigm for the simultaneous installation of mechanical stiffness and high surface hydrophobicity into polymeric organic networks, with the potential for transfer among all porous solids. Control experiments with non-fluorinated congeners underlined the key role of fluorine, in particular, bis-trifluoromethyl functionalization in realizing the dual features of mechanical stiffness and superhydrophobicity.

Introduction

The last decade has observed a striking upsurge of exciting research findings in the realm of porous organic polymers (POPs), due to their remarkably high surface area, low density, feasibility of appending reactive functional moieties at the pore/channel surface, and wide miscellany of framework compositions.[1] The huge application potential for such functionalized materials has been predominantly realised in the domains of molecular storage,[2] heterogeneous catalysis,[3] sensing of molecules/metal ions,[4] selective gas/solvent adsorption,[5] optoelectronics,[6] drug delivery[7] and many others.[8] In this context, gaining insights into the mechanical behaviour for this class of solid-state materials plays a key role to rationally design them for a multitude of technological applications.[2b]

More recently, covalent organic frameworks (COFs) have emerged as a distinctive class of POPs, with extended porous ordered networks bearing open channels constituted by pre-designed organic motifs.[9] The tailored compositions of these lightweight materials confer a unique combination of low mass density, permanent porosity and mechanical robustness.[10] Such relatively underexplored POPs closely resemble the well-studied class of coordination polymers possessing tuneable porosity, that is, metal–organic frameworks (MOFs), whereby the coordination bonds are replaced with strong covalent bonds, with the aim of unification of chemical and structural stability to yield permanent porosity. With parallel but slightly underexplored progress, the field of nitrogen-rich covalent triazine-based frameworks (CTFs) has rapidly flourished to emerge as a vital subclass of COFs,[11] thanks to their excellent thermal stability and chemical inertness.[12] Facile acid-catalysed room-temperature synthesis protocols are an added advantage in the present landscape of promising CTF materials.[13] In the pursuit of incorporating diverse functionalities among CTFs, implementation of suitable material design principles with a view to their intertwined structure–property relationships is considered state-of-the-art.[14] For example, fluorine atoms impart hydrophobicity to the coordination nanospace and result in hydrophobic surface properties.[15] However, the influence of densely packed fluorine atoms on the surface characteristics of COFs and, more precisely, CTFs remains unexplored. Although there are a few reports of studies on the mechanical stiffness of nanoporous MOFs such as isoreticular MOFs (IRMOFs) including MOF-5 (IRMOF-1), HKUST-1 and the prototypal ZIF series,[2b, 16] mechanical behaviour has hitherto

[a] Dr. S. Mukherjee,+ P. Samanta, Dr. S. K. Ghosh
Department of Chemistry
Indian Institute of Science Education and Research (IISER) Pune
Dr. Homi Bhabha Road, Pashan, Pune-411008 (India)
E-mail: sghosh@iiserpune.ac.in

[b] Z. Zeng,+ Dr. A. K. Chaudhari, Dr. J.-C. Tan
Multifunctional Materials & Composites (MMC) Laboratory, Department of Engineering Science, University of Oxford, Parks Road, Oxford OX1 3PJ (UK)
E-mail: jin-chong.tan@eng.ox.ac.uk

[c] Dr. M. M. Shirolkar
Department of Physics, Tamkang University
Tamsui, 251 (Taiwan)

[d] Dr. M. M. Shirolkar
Hefei National Laboratory for Physical Science at the Microscale
University of Science and Technology of China
Hefei, Anhui-230026 (P. R. China)

[e] Dr. S. K. Ghosh
Centre for Energy Science, IISER Pune
Pune-411008 (India)

[+] These authors have contributed equally to this work.

📖 Supporting information and the ORCID identification number(s) for the author(s) of this article can be found under:
https://doi.org/10.1002/chem.201802200.

remained unexplored in organic network architectures such as CTFs.

Lack of crystallinity has largely precluded obtaining adequate structural information on non-crystalline covalent triazine network polymers, often denoted as CTF analogues, despite their diminished framework characteristics.[17] Being amorphous, the latter class often remains elusive in terms of direct observation of structural traits, and experimentally determined porosity serves as their primary fingerprint of characterization.[17] By definition, porous framework materials such as COFs and CTFs have crystallinity.[18] This allows classification of amorphous organic polymers with microporosity under the wider family of POPs, in sync with the chronological development.[19] Traditionally, POPs are categorized as hyper-cross-linked polymers (HCPs),[20] polymers of intrinsic microporosity (PIMs),[21] COFs, CTFs, porous aromatic frameworks (PAFs)[22] and conjugated microporous polymers (CMPs).[23] This nomenclature enables diversely synthesised and functionalised organic network solids to be placed under the all-inclusive category of POPs, subject to upholding the criterion of porosity.[24] Herein, a pair of fluorine-rich POPs based on triazine networks introduce the property of mechanical stiffness among organic network solids. Despite their close resemblance to CTFs, due to their identical building blocks, that is, polynitrile synthetic components undergoing a cyclotrimerisation reaction, the absence of any long-range order delineates the currently reported materials as POPs. Two porous, triazine-based and fluorinated organic polymers, namely, **FPOP-100** and **FPOP-101** (F denotes fluorinated), built from two bis-trifluoromethyl-rich isomeric dinitriles (positional isomers), are presented in this report. The two amorphous FPOPs, owing to surface functionalization of the constituent triazine networks by means of a priori introduction of CF$_3$ groups, show improved hydrophobic properties. Although such highly hydrophobic traits have been realised in congener families of fluorinated porous crystalline networks such as MOFs and imine-based COFs,[15,25] pore surface engineering resulting in superhydrophobic properties among POPs, that is, organic porous network solids, have not been reported

yet. Meanwhile, mechanical properties, in particular, Young's modulus E and hardness H, are of crucial importance to practical uses of materials. Among POPs, dense fluorine-rich environments offer a unique pre-functionalization strategy leading to mechanical stiffness properties comparable to those found in other molecular porous materials, for example, a few zeolites and MOFs.[2b,16,26] Thermal and chemical robustness further widen the applicability of FPOPs under an ample range of operating conditions.

Results and Discussion

Following the room-temperature synthesis protocol of CTFs established by Cooper and co-workers,[13a] fluorous organic porous triazine polymers **FPOP-100** and **FPOP-101** were prepared by acid-catalysed room-temperature reactions of the respective dicyano monomers L′ and L″ in CHCl$_3$ as solvent (Figure 1). Both FPOPs are insoluble in a wide range of organic solvents (DMF, dimethylacetamide, methanol, ethanol, THF, chloroform and hexane) and water. Despite extensive washing, their pronounced insolubility revealed the robust nature of the FPOPs owing to extended network formation coupled with the inherently stable triazine rings.[12c,27] Preparation of the polymeric trimerised compounds was monitored by means of the FTIR spectra of the products (Figure S24 in the Supporting Information). The IR spectra of the two FPOP materials revealed substantial differences when compared to the respective dinitrile precursors L′ and L″, as the C≡N stretching bands of the monomers at 2360 (L′) and 2210 cm^{-1} (L″) were absent in the resulting POPs, as shown in Figure S24 of the Supporting Information. Furthermore, characteristic peaks for the triazine ring at about 1520 (**FPOP-100**) and 1500 cm^{-1} (**FPOP-101**) appeared, suggestive of cyclotrimerised functionality in each of them. Thermogravimetric analysis (TGA) under N$_2$ atmosphere for the as-synthesized phases showed an initial loss of about 10% of guest solvent species occluded during the syntheses followed by negligible weight loss up to about 300 (**FPOP-100**) and about 315 °C (**FPOP-101**) (Figures S18 and S19 in the
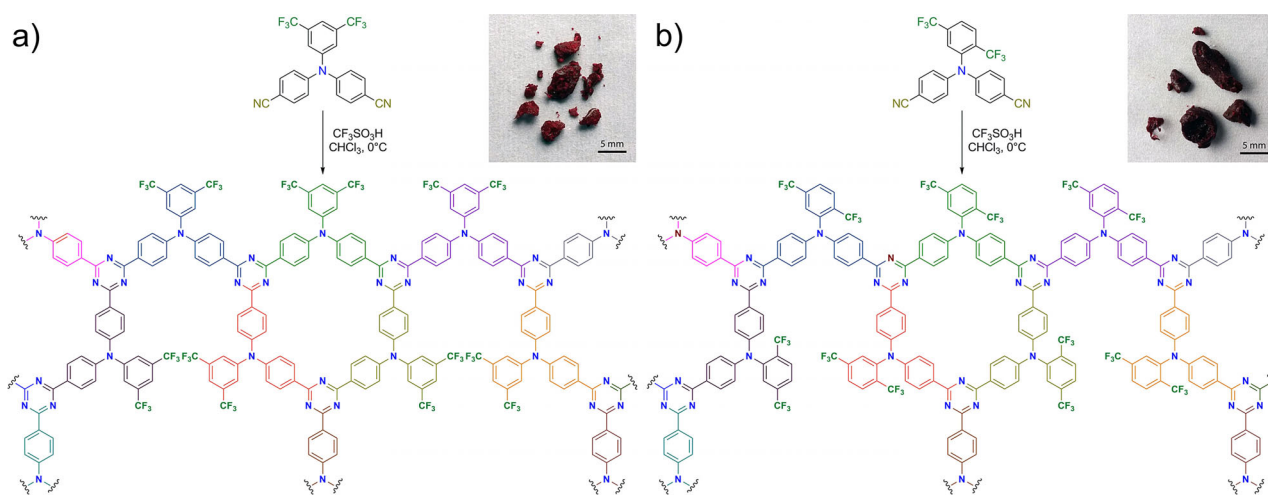

Figure 1. Schematic syntheses of the fluorinated organic polymers. a) **FPOP-100** from L′ and b) **FPOP-101** from L″. Insets show the mechanically stiff monolithic compounds **FPOP-100** and **FPOP-101**, respectively.

◥◥ These are not the final page numbers!

Supporting Information). A complementary thermoanalytical study was done by differential scanning calorimetry (DSC, Figure S34 in the Supporting Information). Typical guest-exchange protocols with lower-boiling solvents (chloroform and THF, 1:1 binary mixture) followed by evacuation under vacuum resulted in complete desolvation of the compounds, since both the ensuing guest-free POP phases were found to suffer no weight loss up to about 300 °C. On the contrary, thermal stabilities of the corresponding monomer building blocks L' and L'' were relatively poor (Figures S18 and S19 in the Supporting Information), as is typical for such organic dinitrile monomers.

The powder XRD patterns of both FPOPs (as-synthesized and guest-free phases) showed amorphous nature (Figure 2 d). However, the broad diffraction peaks observed at $2\theta = 18.4$ and $19.5°$ for **FPOP-100** and **FPO-101**, respectively, suggested the existence of graphitic 2D layers. Such broad diffraction patterns hinder precise structure elucidation due to the absence of any long-range order in the bulk FPOPs. However, weak crystalline nature is often observed in POPs, especially in triazine network polymers prepared by room-temperature methods.[13] In fact, this suggests that our glassy polymer materials may consist of non-coplanar, 2D organic layers; that is, aromatic networks beyond any repeatable pattern, resembling hard carbon.[28]

Low-temperature (195 K) CO_2 adsorption isotherms for **FPOP-100** and **FPOP-101** afforded BET surface areas of 261 and 274 $m^2 g^{-1}$, respectively, corresponding to pore volumes of about 0.1 $cm^3 g^{-1}$ for both. The respective saturation uptake capacities of 92 and 94 $cm^3 g^{-1}$ (Figures 2 a and b) imply extrinsic porosity. The N_2 and H_2 adsorption isotherms recorded at 77 K exhibit small uptakes of 27 and 6 $cm^3 g^{-1}$ (N_2) and 43 and 41 $cm^3 g^{-1}$ (H_2) for **FPOP-100** and **FPOP-101**, respectively (Fig-

ures 2 a and b). Pore size distributions derived from the CO_2 isotherms, that is, Horvath–Kawazoe plots, for both polymers showed ultramicropores (< 7 Å) of uniform width (≈ 5 Å, Figure 2 c). Such low-porosity signatures are in accord with their observed amorphous nature, as a consequence of irregular packing among the constituent polymeric triazine networks. However, more importantly, the physisorption experiments lead one to conclude porosity for the POPs.

Solid-state ^{13}C CP-MAS NMR spectra showed a characteristic peak for the triazine ring carbon atoms at about 174 ppm and other peaks between 100 and 240 ppm, which correspond to the different aromatic carbon atoms, as labelled in Figure S28 in the Supporting Information: six types of carbon atoms for **FPOP-100** (b–g), and seven types for **FPOP-101** (b–h). The FESEM images show that the stiff FPOP samples are dense aggregates of particles forming similar homogeneous nanospheres (Figures S20 and S21 in the Supporting Information). Similar homogeneous nanosphere morphology was also revealed in the AFM images (3D and roughness) of the triazine-based polymeric networks, as shown in Figures S22 and S23 of the Supporting Information. AFM morphological analyses also revealed that the average diameters of **FPOP-100** and **FPOP-101** nanospheres lie in very close range (330 and 240 nm, respectively), and thus reveal comparable physical traits for the two **FPOP**s, possibly traceable to their isomeric precursors. Comparative analysis of the Raman spectra of the dinitrile monomers as well as the two FPOPs revealed the disappearance of the C≡N stretching bands at $\tilde{\nu}(C≡N) \approx 2220–2230$ cm^{-1} (Figure S27 in the Supporting Information) and simultaneously disclosed similar network architectures of **FPOP-100** and **FPOP-101**, evidenced by the similarity between their corresponding rotational-vibrational spectral signatures.
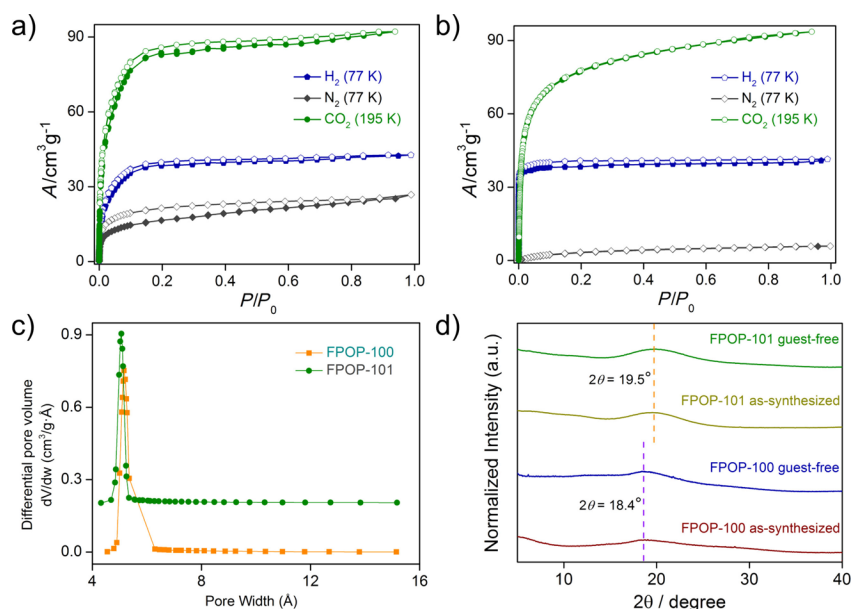

Figure 2. a), b) Low-temperature CO_2, N_2 and H_2 adsorption isotherms for **FPOP-100** and **FPOP-101**; closed and open symbols represent adsorption and desorption, respectively. c) Horvath–Kawazoe pore size distribution profiles of FPOPs, calculated from CO_2 isotherms (195 K). d) Powder XRD patterns of as-synthesized and guest-free phases of FPOPs. The broad diffraction peaks at $2\theta = 18.4$ (**FPOP-100**) and $19.5°$ (**FPOP-101**) indicate the existence of 2D layers in the polymers.

These are not the final page numbers! ↗↗

Fluorinated porous networks such as fluorinated MOFs have been recognised in the recent literature to exhibit excellent water repellence alongside affinity toward hydrocarbon vapours such as benzene.[15, 25a, 29] As evidence of the fluorine-dense nature, water-vapour sorption isotherm experiments with the FPOPs showed negligible uptake, even under saturation vapour pressure of water (3.17 kPa at 298 K), whereas hydrophobic oil-constituent hydrocarbon benzene showed slow opening-assisted high saturation uptake profiles (Figures 3 a
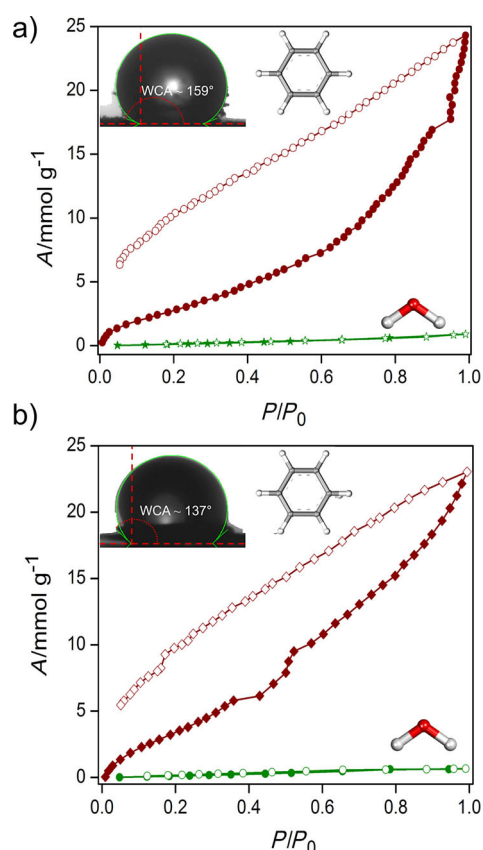

Figure 3. Contrasting water (green) and benzene (burgundy) vapour sorption isotherms for a) **FPOP-100** and b) **FPOP-101**. Closed and open symbols denote adsorption and desorption, respectively. Insets: Images of water drops slowly cast on the water-repellent surfaces of **FPOP-100** and **FPOP-101** pellets with superhydrophobic and highly hydrophobic WCAs of about 159 and 137°, respectively.

and b). The stepwise nature of these benzene sorption isotherms suggest enhanced host–guest interactions with more and more surface accumulation of the benzene-vapour sorbate. In the case of densely cross-linked polymers like these, having very narrow openings (as suggested by the gas sorption isotherms), such a hydrocarbon-vapour sorption isotherm suggests a possible role of slow filling of the fluorous voids assisted by the confinement effect.[15a, 30] Moreover, the contrasting vapour-sorption isotherms (water and C_6 hydrocarbon benzene) correlates with the anticipated hydrophobicity of the FPOP materials. Subsequently, the surface-wetting properties

of the bulk amorphous phases were assessed by measurements of water contact angle (WCA). These experiments reproducibly registered static water contact angles as high as 159 and 137° for **FPOP-100** and **FPOP-101**, respectively (with sessile drops), which evidenced a highly hydrophobic nature for both; **FPOP-100** even reached superhydrophobicity. In fact, the aforesaid high WCAs rank these two POPs among only a few hydrophobic porous organic polymers hitherto reported.[25b, 31]

Using instrumented nanoindentation, we found that Young's modulus E and hardness H of **FPOP-100** are 3.4 ± 0.2 GPa (assuming that the Poisson's ratio is 0.3) and 230 ± 20 MPa, respectively. The E and H values of **FPOP-101** are 3.3 ± 0.3 GPa and 290 ± 40 MPa, respectively. Thus, **FPOP-100** with CF_3 groups in the 3,5-positions has a comparable level of stiffness but considerably lower hardness relative to **FPOP-101**, which has CF_3 groups in the 2,5-positions. A plausible explanation for the lower stiffness of **FPOP-101** is the wider angle between CF_3 groups, as this might affect the network packing. In addition, under identical loading conditions, **FPOP-100** exhibits less creep-induced deformation than **FPOP-101** (Figure 4b). Scattering in the E (Figure 4c) and H data (Figure 4d) is most likely due to microstructural inhomogeneity, that is, non-uniformly distributed porosity. At the shallow indentation of less than about 250 nm in this study, E and H are overestimated because the Berkovich indenter is not perfectly sharp, and thus at the tip apex the actual contact area is larger than the assumed ideal value. Therefore, E and H values were determined by averaging the values after indenting to 500 nm.

Many factors could interfere with the accurate measurement of contact area (such as subsurface cracking) and influence the recovery of the material resulting in a distorted unloading curve (e.g., creep effect).[17b] Figure 4d shows that H is unaffected by increasing indentation depth, and this suggests that no appreciable subsurface cracks are generated after indenting to 2 μm. The descending trend of E could be attributed to microstructural inhomogeneities of **FPOP-100** and **FPOP-101**. Under an optical microscope, **FPOP-101** sample shows more non-uniformly distributed micropores than **FPOP-100**, and this is further reflected in the higher N_2 uptakes as well as the higher creep rate (Figure 4b) of **FPOP-101**.

As shown in the materials selection map (Figure 5),[2b, 26] Young's moduli and hardness of **FPOP-100** and **FPOP-101** resemble those of zeolitic imidazolate frameworks (ZIFs),[32] which are an important family of MOFs and are isomorphic with zeolites from the topological perspective. The correlation of Young's moduli and densities of the FPOPs was further investigated for comparison with ZIFs and ten other common polymers. Densities ρ of **FPOP**s were measured by using a Mettler Toledo instrument on the basis of the Archimedes principle. The densities of **FPOP-100** ($\rho = 1440.03 \pm 46.29$ kg m^{-3}) and **FPOP-101** ($\rho = 1451.61 \pm 20.67$ kg m^{-3}) are higher than that of ZIF-8 (Figure 6), which has nearly the same E but higher H (H{110} of ZIF-8: 531 ± 28 MPa).[26, 33] This higher hardness of ZIF-8 indicates its ability to withstand higher load when the projected area of residual impression stays the same for both ZIF-8 and FPOPs. In other words, under the same indentation
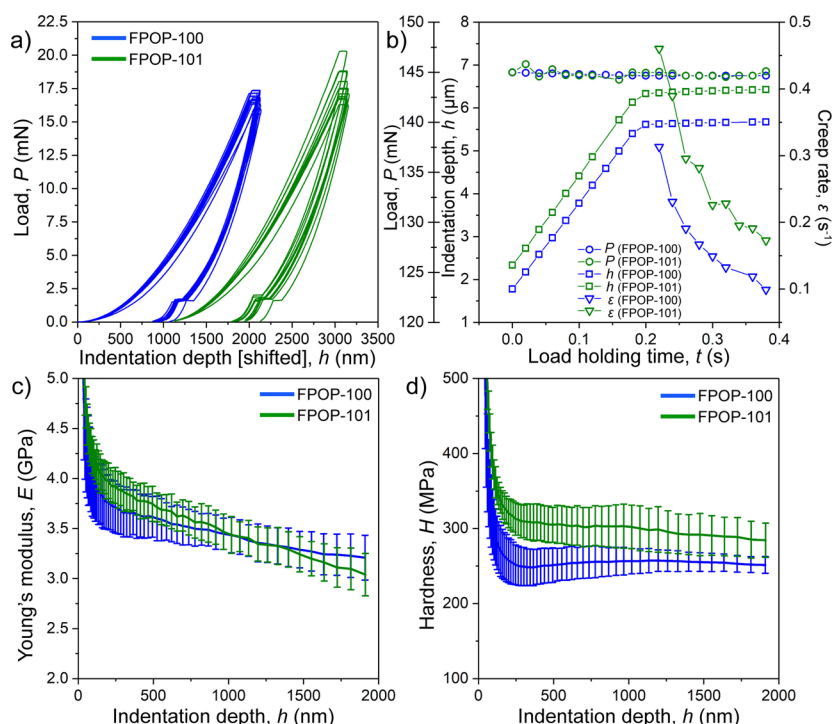
↖↖ These are not the final page numbers!

Figure 4. MTS nanoindentation of FPOPs. a) Load versus deformation curves. b) Creep tests by applying cyclic impact (Figure S33 in the Supporting Information). c) Young's modulus and d) hardness versus indentation depth.
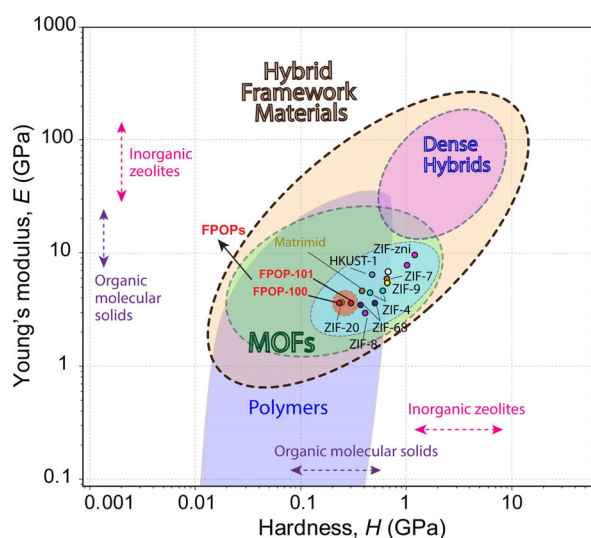

Figure 5. Young's modulus E versus hardness H with classified materials property map.[2b] The E and H values of **FPOP-100** and **FPOP-101** are similar to those of MOFs such as ZIFs and glassy polymers such as Matrimid.

Figure 6. Plot of Young's modulus E versus density ρ showing the correlation between E and ρ for FPOPs, ZIFs and ten common polymers.[2b]

load, FPOPs suffer more permanent deformation, which could be plastic deformation of the network until eventual bond breakage.

Using the MTS nanoindenter, we applied cyclic loads to the FPOPs to continuously deform their surfaces. During the cyclic impact study, compaction of the networks occurs, which is reflected in Figure 7, where the energy loss decreases with increasing number of loading cycles (see Table 1 for energy lost at the first impact cycle). We found that **FPOP-100** is tougher
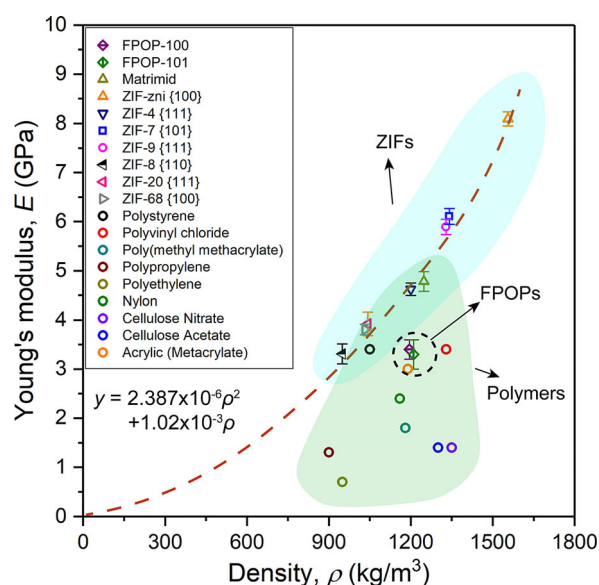
than **FPOP-101**, because the energy of mechanical deformation of **FPOP-100** in the first approximately 15 impact cycles is apparently higher than that of **FPOP-101**. Nevertheless, energy lost per impact cycle converges to about 429 nJ after approximately 40 cycles, and this suggests gradual rupture of most of the CF$_3$ groups in both **FPOP-100** and **FPOP-101** leads to material compaction reminiscent of that of ductile polymers. Further information on the loading conditions is shown in the
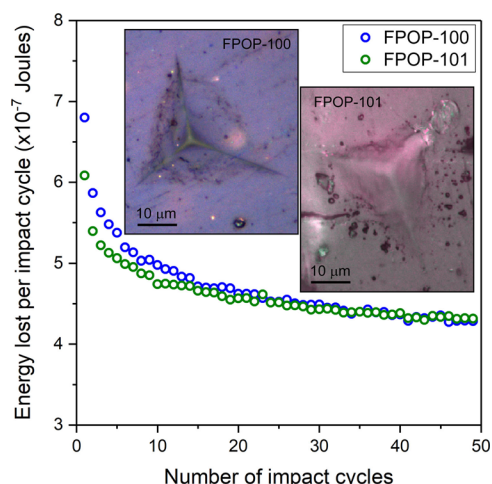
Figure 7. Energy dissipated per impact cycle versus the number of cycles showing the relative toughness of **FPOP-100** and **FPOP-101**. Optical images of the residual impressions on **FPOP-100** and **FPOP-101** are shown in the insets.

Table 1. Energy dissipation at the first impact cycle (assuming the volume is the Berkovich indenter volume under the sample surface at maximum depth).

	FPOP-100	FPOP-101
Energy lost per unit volume [$\times 10^8$ J m^{-3}]	4.59	3.48
Energy lost per unit mass [kJ g^{-1}]	0.32	0.24

Supporting Information (Figure S33 in the Supporting Information).

Control experiments were performed to understand the role of fluorine atoms in inducing hydrophobicity and mechanical stiffness. For verification purposes, the substituents of the dinitrile precursors were fine-tuned: CF$_3$ groups in L′ and L″ were replaced by CH$_3$ and H atoms to afford three differently substituted dinitrile building blocks (L$_1$: 4,4′-(3,5- dimethylphenylazanediyl)dibenzonitrile; L$_2$: 4,4′-(2,5-dimethylphenylazanediyl)dibenzonitrile; L$_3$: 4,4′-(phenylazanediyl)dibenzonitrile) for making an analogous series of non-fluorinated POPs **MPOP-100**, **MPOP-101** and **POP-100**, respectively (Figures S9–S17, S29 and S30 in the Supporting Information). Photographs of these three materials (insets to Figures S29a–c in the Supporting Information) showed the physical appearances of typical powdered materials devoid of mechanical stiffness and thus unable to form a bulk monolith. Since dinitriles L$_2$ and L$_3$ remained amorphous despite a number of crystallisation attempts, the crystal packing of L$_1$ was considered as representative of the three non-fluorinated precursors. A closer look at the intermolecular packing modes, in which intermolecular H-bonding and van der Waals interactions are evident, reveals contrasting natures of such interactions (manifold for L′ and L″ but merely onefold for L$_1$, considering a single unit cell (1×1×1) for each; Figures S25 and S26 in the Supporting Information). Such multiple interactions mediated by C—F bonds may play a key role in augmenting the extended cross-linking in the densely packed and fluorinated triazine polymer motifs. To

support these analyses from a more practical viewpoint, we measured the static water contact angles with sessile drops for all three non-fluorinated POPs (Figure S32 in the Supporting Information) and found hydrophilic nature for all the three surfaces. When these low WCAs are contrasted against the high superhydrophobic surface characteristics manifested by **FPOP-100** and **FPOP-101** surfaces, the pivotal role of bis-trifluoromethyl functionalization becomes evident.

Conclusions

Installation of bis-trifluoromethyl functionalisation is an interesting avenue to develop self-assembled, hydrophobic FPOPs. Mechanical studies have established that their stiffness behaviour is analogous to those of their organic–inorganic hybrid polymer congeners, particularly ZIFs, and glassy polymers, whereas surface hydrophobicity measurements revealed the role of CF$_3$ groups in the observed superhydrophobicity. The present study offers a new paradigm to simultaneously introduce mechanical stiffness and high surface hydrophobicity into polymeric organic networks and may serve as a roadmap to guide the engineering of a future generation of mechanically stiff and hydrophobic materials.

Experimental Section

Materials

4-Fluorobenzonitrile (99%), caesium fluoride (99%) and trifluoromethanesulfonic acid (reagent grade, 98%) were purchased from Sigma-Aldrich. Dry and HPLC-grade solvents (including DMF) were obtained from Alfa Aesar. 3,5-Bis(trifluoromethyl)aniline ($>$97%), 2,5-bis(trifluoromethyl)aniline ($>$98%), 3,5-dimethylaniline ($>$98%) and 2,5-dimethylaniline ($>$97%) were procured from TCI Chemicals. These chemicals were used without further purification.

Physical measurements

The IR spectra were recorded with NICOLET 6700 FTIR spectrophotometer by using KBr pellets in the 600–3000 cm^{-1} range. TGA data were recorded with PerkinElmer STA 6000 TGA analyser under N$_2$ atmosphere with heating rate of 10°C min^{-1}. Gas adsorption measurements were performed with a BelSorp-max instrument from Bel Japan. Contact angles on **FPOP-100** and **FPOP-101** were measured with a contact-angle meter (Model ID: HO-IAD-CAM-01; Holmarc Opto-Mechatronics Pvt. Ltd.), followed by LBADSA drop analysis (ImageJ software), which is based on the fitting of the Young–Laplace equation to the droplet image data (droplet shape analysis), by using 10 μL of distilled water, with an accuracy of $\pm 2°$. The morphologies of the POP samples were recorded with a Zeiss Ultra Plus FESEM. Powder PXRD data were recorded at room temperature with a Bruker D8 Advance diffractometer by using Cu$_{K\alpha}$ radiation ($\lambda = 1.5406$ Å). Raman spectra ($\lambda_{exc} = 532$ nm) were recorded with a Raman microscope (LabRAM HR, Horbia Jobin Yvon) with a 60× objective lens. The morphologies of the FPOP nanospheres were characterised by AFM (Agilent Keysight 5500 AFM). The measurements were performed in non-contact mode by using an Si tip with tip resonance frequency of 330 kHz and cantilever thickness of 4 μm. Solid-state ^{13}C CP-MAS NMR spectra were recorded with a Bruker Advance-III Ultrashield500WB spectrometer (probe: MAS BB 4MM, spinning rate: 5KHz) with guest-free POP

samples (crushed and packed tightly in quartz capillaries), whereas liquid-state NMR characterization of dinitrile precursors were performed with a 400 MHz Jeol ECS-400 (or 100 MHz for ^{13}C) and 270 MHz JEOL FX-270 NMR (or 67.5 MHz for ^{13}C) spectrometers.

X-ray structural studies

Single-crystal X-ray data of precursors L′ and L′′ were collected at 150 K with a Bruker D8 Quest diffractometer (operated at 1500 W power: 50 kV, 30 mA) by using graphite-monochromated Mo$_{K\alpha}$ radiation ($\lambda = 0.71073$ Å). Crystals were mounted on nylon CryoLoops (Hampton Research) with Paratone-N (Hampton Research). The data integration and reduction were processed with SAINT[34] software and the Olex2[35] package. A multiscan absorption correction was applied to the collected reflections. The structure was solved by direct methods with SHELXTL[36] and was refined on F^2 by full-matrix least-squares techniques with the SHELXL-97[37] program package within the WINGX[38] programme. All non-hydrogen atoms were anisotropically refined. All hydrogen atoms were located in successive difference Fourier maps and they were treated as riding atoms by using SHELXL default parameters. Both the structures were examined using the *Adsym* subroutine of PLATON[39] to assure that no additional symmetry could be applied to the models.

CCDC 1823779 (L′), 1823780 (L′′) and 1823781 (L$_1$) contain the supplementary crystallographic data for this paper. These data are provided free of charge by The Cambridge Crystallographic Data Centre.

Low-pressure gas and solvent sorption measurements

Low pressure gas and solvent sorption measurements were performed with BELSORP-max and BELSORP-aqua3 adsorption analysers (BEL Japan, Inc.), respectively, both equipped with a constant-temperature bath. All the employed gases were of 99.99% purity, and the solvents were of HPLC grade. THF/CHCl$_3$ (1:1)-exchanged phases of the **FPOP-100** and **FPOP-101** were heated at 80 °C under vacuum for 2 h to get guest-free phases of the respective polymers. Prior to each adsorption measurement, the guest-free samples were again pre-treated at 80 °C under vacuum for 1 h, by using a BelPrepvacII instrument, and purged with N$_2$ on cooling. All solvent sorption measurements were recorded at 298 K.

Nanoindentation

Nanoindentation experiments were implemented with an MTS NanoIndenter XP, which is a microprobe instrument for measuring mechanical properties. This system is able to measure the interface contact stiffness continuously during each indentation. A Berkovich indenter (three-sided pyramidal indenter, apex radius ≈ 100 nm) was adopted to measure Young's modulus and hardness. It can also be used to generate cracks for measuring fracture toughness because it is sharper than a spherical indenter,[40] which is apt to cause stable elastic–plastic transition rather than inducing cracks. An array of instrumented indentations of about 2 µm depth was implemented on both **FPOP-100** and **FPOP-101**, which were mounted on epoxy resin and then polished with a suspension of polycrystalline diamond (crystals diameter ≈ 0.1 µm) to achieve efficient cutting and minimal deformation.

Conflict of interest

The authors declare no conflict of interest.

[1] a) J.-X. Jiang, A. I. Cooper in *Functional Metal-Organic Frameworks: Gas Storage, Separation and Catalysis* (Ed.: M. Schröder), Springer, Berlin, Heidelberg, **2010**, pp. 1–33; b) Y. Xu, S. Jin, H. Xu, A. Nagai, D. Jiang, *Chem. Soc. Rev.* **2013**, *42*, 8012–8031; c) D. Wu, F. Xu, B. Sun, R. Fu, H. He, K. Matyjaszewski, *Chem. Rev.* **2012**, *112*, 3959–4015; d) E. Merino, E. Verde-Sesto, E. M. Maya, M. Iglesias, F. Sánchez, A. Corma, *Chem. Mater.* **2013**, *25*, 981–988; e) P. Samanta, P. Chandra, A. V. Desai, S. K. Ghosh, *Mater. Chem. Front.* **2017**, *1*, 1384–1388.

[2] a) C. R. DeBlase, K. E. Silberstein, T.-T. Truong, H. D. Abruña, W. R. Dichtel, *J. Am. Chem. Soc.* **2013**, *135*, 16821–16824; b) J. C. Tan, A. K. Cheetham, *Chem. Soc. Rev.* **2011**, *40*, 1059–1080.

[3] a) H. Xu, J. Gao, D. Jiang, *Nat. Chem.* **2015**, *7*, 905–912; b) Y. Peng, Z. Hu, Y. Gao, D. Yuan, Z. Kang, Y. Qian, N. Yan, D. Zhao, *ChemSusChem* **2015**, *8*, 3208–3212; c) M. H. Alkordi, L. J. Weselinski, V. D'Elia, S. Barman, A. Cadiau, M. N. Hedhili, A. J. Cairns, R. G. AbdulHalim, J.-M. Basset, M. Eddaoudi, *J. Mater. Chem. A* **2016**, *4*, 7453–7460.

[4] a) S. Wan, J. Guo, J. Kim, H. Ihee, D. Jiang, *Angew. Chem. Int. Ed.* **2008**, *47*, 8826–8830; *Angew. Chem.* **2008**, *120*, 8958–8962; b) S. Dalapati, E. Jin, M. Addicoat, T. Heine, D. Jiang, *J. Am. Chem. Soc.* **2016**, *138*, 5797–5800; c) D. Gopalakrishnan, W. R. Dichtel, *J. Am. Chem. Soc.* **2013**, *135*, 8357–8362; d) J. Dong, K. Zhang, X. Li, Y. Qian, H. Zhu, D. Yuan, Q.-H. Xu, J. Jiang, D. Zhao, *Nat. Commun.* **2017**, *8*, 1142.

[5] a) A. Karmakar, A. Kumar, A. K. Chaudhari, P. Samanta, A. V. Desai, R. Krishna, S. K. Ghosh, *Chem. Eur. J.* **2016**, *22*, 4931–4937; b) C. J. Doonan, D. J. Tranchemontagne, T. G. Glover, J. R. Hunt, O. M. Yaghi, *Nat. Chem.* **2010**, *2*, 235–238; c) S. Hug, L. Stegbauer, H. Oh, M. Hirscher, B. V. Lotsch, *Chem. Mater.* **2015**, *27*, 8001–8010.

[6] a) H. Takeda, M. Ohashi, Y. Goto, T. Ohsuna, T. Tani, S. Inagaki, *Chem. Eur. J.* **2014**, *20*, 9130–9136; b) K. Schwinghammer, S. Hug, M. B. Mesch, J. Senker, B. V. Lotsch, *Energy Environ. Sci.* **2015**, *8*, 3345–3353; c) V. S. Vyas, F. Haase, L. Stegbauer, G. Savasci, F. Podjaski, C. Ochsenfeld, B. V. Lotsch, *Nat. Commun.* **2015**, *6*, 8508.

[7] a) Q. Fang, J. Wang, S. Gu, R. B. Kaspar, Z. Zhuang, J. Zheng, H. Guo, S. Qiu, Y. Yan, *J. Am. Chem. Soc.* **2015**, *137*, 8352–8355; b) L. Bai, S. Z. F. Phua, W. Q. Lim, A. Jana, Z. Luo, H. P. Tham, L. Zhao, Q. Gao, Y. Zhao, *Chem. Commun.* **2016**, *52*, 4128–4131.

[8] a) T. Uemura, T. Kaseda, Y. Sasaki, M. Inukai, T. Toriyama, A. Takahara, H. Jinnai, S. Kitagawa, *Nat. Commun.* **2015**, *6*, 7473; b) P. J. Waller, F. Gándara, O. M. Yaghi, *Acc. Chem. Res.* **2015**, *48*, 3053–3063; c) Y.-B. Huang, P. Pachfule, J.-K. Sun, Q. Xu, *J. Mater. Chem. A* **2016**, *4*, 4273–4279.

[9] a) C. S. Diercks, O. M. Yaghi, *Science* **2017**, *355*, eaal1585; b) S. Wan, J. Guo, J. Kim, H. Ihee, D. Jiang, *Angew. Chem. Int. Ed.* **2009**, *48*, 5439–5442; *Angew. Chem.* **2009**, *121*, 5547–5550; c) P. Samanta, A. V. Desai, B. Anothumakkool, M. M. Shirolkar, A. Karmakar, S. Kurungot, S. K. Ghosh, *J. Mater. Chem. A* **2017**, *5*, 13659–13664.

[10] Q. Sun, B. Aguila, J. Perman, L. D. Earl, C. W. Abney, Y. Cheng, H. Wei, N. Nguyen, L. Wojtas, S. Ma, *J. Am. Chem. Soc.* **2017**, *139*, 2786–2793.

[11] K. Wang, L. M. Yang, X. Wang, L. Guo, G. Cheng, C. Zhang, S. Jin, B. Tan, A. Cooper, *Angew. Chem. Int. Ed.* **2017**, *56*, 14149–14153; *Angew. Chem.* **2017**, *129*, 14337–14341.

[12] a) P. Kuhn, M. Antonietti, A. Thomas, *Angew. Chem. Int. Ed.* **2008**, *47*, 3450–3453; *Angew. Chem.* **2008**, *120*, 3499–3502; b) Y. Zhao, K. X. Yao, B. Teng, T. Zhang, Y. Han, *Energy Environ. Sci.* **2013**, *6*, 3684–3692; c) S.
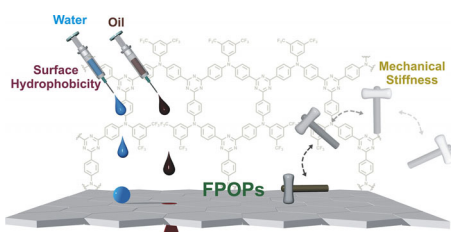
Kuecken, J. Schmidt, L. Zhi, A. Thomas, *J. Mater. Chem. A* **2015**, *3*, 24422–24427.

[13] a) S. Ren, M. J. Bojdys, R. Dawson, A. Laybourn, Y. Z. Khimyak, D. J. Adams, A. I. Cooper, *Adv. Mater.* **2012**, *24*, 2357–2361; b) X. Zhu, C. Tian, S. M. Mahurin, S.-H. Chai, C. Wang, S. Brown, G. M. Veith, H. Luo, H. Liu, S. Dai, *J. Am. Chem. Soc.* **2012**, *134*, 10478–10484; c) C. E. Chan-Thaw, A. Villa, P. Katekomol, D. Su, A. Thomas, L. Prati, *Nano Lett.* **2010**, *10*, 537–541; d) L. Hao, J. Ning, B. Luo, B. Wang, Y. Zhang, Z. Tang, J. Yang, A. Thomas, L. Zhi, *J. Am. Chem. Soc.* **2015**, *137*, 219–225; e) R. Palkovits, M. Antonietti, P. Kuhn, A. Thomas, F. Schüth, *Angew. Chem. Int. Ed.* **2009**, *48*, 6909–6912; *Angew. Chem.* **2009**, *121*, 7042–7045; f) H. Liao, H. Ding, B. Li, X. Ai, C. Wang, *J. Mater. Chem. A* **2014**, *2*, 8854–8858.

[14] a) Z.-F. Pang, S.-Q. Xu, T.-Y. Zhou, R.-R. Liang, T.-G. Zhan, X. Zhao, *J. Am. Chem. Soc.* **2016**, *138*, 4710–4713; b) M. Tong, Q. Yang, Y. Xiao, C. Zhong, *Phys. Chem. Chem. Phys.* **2014**, *16*, 15189–15198; c) Y. Zeng, R. Zou, Y. Zhao, *Adv. Mater.* **2016**, *28*, 2855–2873.

[15] a) S. Mukherjee, A. M. Kansara, D. Saha, R. Gonnade, D. Mullangi, B. Manna, A. V. Desai, S. H. Thorat, P. S. Singh, A. Mukherjee, S. K. Ghosh, *Chem. Eur. J.* **2016**, *22*, 10937–10943; b) T.-H. Chen, I. Popov, O. Zenasni, O. Daugulis, O. S. Miljanic, *Chem. Commun.* **2013**, *49*, 6846–6848.

[16] D. F. Bahr, J. A. Reid, W. M. Mook, C. A. Bauer, R. Stumpf, A. J. Skulan, N. R. Moody, B. A. Simmons, M. M. Shindel, M. D. Allendorf, *Phys. Rev. B* **2007**, *76*, 184106.

[17] a) H. Ma, H. Ren, S. Meng, F. Sun, G. Zhu, *Sci. Rep.* **2013**, *3*, 2611; b) L.-M. Tao, F. Niu, D. Zhang, T.-M. Wang, Q.-H. Wang, *New J. Chem.* **2014**, *38*, 2774–2777; c) F. Niu, L. Tao, Y. Deng, H. Gao, J. Liu, W. Song, *New J. Chem.* **2014**, *38*, 5695–5699; d) K. Sakaushi, G. Nickerl, F. M. Wisser, D. Nishio-Hamane, E. Hosono, H. Zhou, S. Kaskel, J. Eckert, *Angew. Chem. Int. Ed.* **2012**, *51*, 7850–7854; *Angew. Chem.* **2012**, *124*, 7972–7976.

[18] X. Feng, X. Ding, D. Jiang, *Chem. Soc. Rev.* **2012**, *41*, 6010–6022.

[19] S. Yuan, B. Dorney, D. White, S. Kirklin, P. Zapol, L. Yu, D.-J. Liu, *Chem. Commun.* **2010**, *46*, 4547–4549.

[20] V. A. Davankov, M. P. Tsyurupa, *React. Polym.* **1990**, *13*, 27–42.

[21] P. M. Budd, B. S. Ghanem, S. Makhseed, N. B. McKeown, K. J. Msayib, C. E. Tattershall, *Chem. Commun.* **2004**, 230–231.

[22] T. Ben, H. Ren, S. Ma, D. Cao, J. Lan, X. Jing, W. Wang, J. Xu, F. Deng, J. M. Simmons, S. Qiu, G. Zhu, *Angew. Chem. Int. Ed.* **2009**, *48*, 9457–9460; *Angew. Chem.* **2009**, *121*, 9621–9624.

[23] a) J. X. Jiang, F. Su, A. Trewin, C. D. Wood, N. L. Campbell, H. Niu, C. Dickinson, A. Y. Ganin, M. J. Rosseinsky, Y. Z. Khimyak, A. I. Cooper, *Angew. Chem. Int. Ed.* **2007**, *46*, 8574–8578; *Angew. Chem.* **2007**, *119*, 8728–8732; b) A. I. Cooper, *Adv. Mater.* **2009**, *21*, 1291–1295.

[24] R. Dawson, A. I. Cooper, D. J. Adams, *Prog. Polym. Sci.* **2012**, *37*, 530–563.

[25] a) Z.-R. Jiang, J. Ge, Y.-X. Zhou, Z. U. Wang, D. Chen, S.-H. Yu, H.-L. Jiang, *NPG Asia Mater.* **2016**, *8*, e253; b) D. Mullangi, S. Shalini, S. Nandi, B. Choksi, R. Vaidhyanathan, *J. Mater. Chem. A* **2017**, *5*, 8376–8384.

[26] J. C. Tan, T. D. Bennett, A. K. Cheetham, *Proc. Natl. Acad. Sci. USA* **2010**, *107*, 9938–9943.

[27] P. Puthiaraj, Y.-R. Lee, S. Zhang, W.-S. Ahn, *J. Mater. Chem. A* **2016**, *4*, 16288–16311.

[28] a) K. Sakaushi, E. Hosono, G. Nickerl, H. Zhou, S. Kaskel, J. Eckert, *J. Power Sources* **2014**, *245*, 553–556; b) T. Zheng, W. Xing, J. R. Dahn, *Carbon* **1996**, *34*, 1501–1507.

[29] S.-I. Noro, T. Nakamura, *NPG Asia Mater.* **2017**, *9*, e433.

[30] C. Yang, U. Kaipa, Q. Z. Mather, X. Wang, V. Nesterov, A. F. Venero, M. A. Omary, *J. Am. Chem. Soc.* **2011**, *133*, 18094–18097.

[31] D.-P. Liu, Q. Chen, Y.-C. Zhao, L.-M. Zhang, A.-D. Qi, B.-H. Han, *ACS Macro Lett.* **2013**, *2*, 522–526.

[32] a) R. Banerjee, A. Phan, B. Wang, C. Knobler, H. Furukawa, M. O'Keeffe, O. M. Yaghi, *Science* **2008**, *319*, 939–943; b) S. El-Hankari, J. Aguilera-Sigalat, D. Bradshaw, *J. Mater. Chem. A* **2016**, *4*, 13509–13518.

[33] Z. Zeng, J.-C. Tan, *ACS Appl. Mater. Interfaces* **2017**, *9*, 39839–39854.

[34] SAINT Plus, (Version 7.03); Bruker AXS Inc.: Madison, WI, **2004**.

[35] O. V. Dolomanov, L. J. Bourhis, R. J. Gildea, J. A. K. Howard, H. Puschmann, *J. Appl. Crystallogr.* **2009**, *42*, 339–341.

[36] G. M. Sheldrick, SHELXTL, Reference Manual: version 5.1: Bruker AXS; Madison, WI, **1997**.

[37] G. Sheldrick, *Acta Crystallogr. Sect. A* **2008**, *64*, 112–122.

[38] WINGX version 1.80.05 Louis Farrugia, University of Glasgow.

[39] A. L. Spek, PLATON, A Multipurpose Crystallographic Tool, Utrecht University, Utrecht, The Netherlands, **2005**.

[40] J. C. Tan, C. A. Merrill, J. B. Orton, A. K. Cheetham, *Acta Mater.* **2009**, *57*, 3481–3496.

↖↖ These are not the final page numbers!

FULL PAPER

CHEMISTRY
A European Journal
Full Paper

ChemPubSoc
Europe

FPOPs hit: Fluorous organic building blocks were used to develop self-assembled, hydrophobic, fluorinated porous organic polymers **FPOP-100** and **FPOP-101**. These functionalized triazine network polymers show mechanical stiffness similar to those of metal–organic frameworks and high surface hydrophobicity (see figure).

These are not the final page numbers! ↗↗